WPMST1-PR(17) 18303

B Vanovac et al.

Effects of density gradients and fluctuations at the plasma edge on ECEI measurements at ASDEX Upgrade

Preprint of Paper to be submitted for publication in
Plasma Physics and Controlled Fusion

This work has been carried out within the framework of the EUROfusion Consortium and has received funding from the Euratom research and training programme 2014-2018 under grant agreement No 633053. The views and opinions expressed herein do not necessarily reflect those of the European Commission.

This document is intended for publication in the open literature. It is made available on the clear understanding that it may not be further circulated and extracts or references may not be published prior to publication of the original when applicable, or without the consent of the Publications Officer, EUROfusion Programme Management Unit, Culham Science Centre, Abingdon, Oxon, OX14 3DB, UK or e-mail Publications.Officer@euro-fusion.org

Enquiries about Copyright and reproduction should be addressed to the Publications Officer, EUROfusion Programme Management Unit, Culham Science Centre, Abingdon, Oxon, OX14 3DB, UK or e-mail Publications.Officer@euro-fusion.org

The contents of this preprint and all other EUROfusion Preprints, Reports and Conference Papers are available to view online free at http://www.euro-fusionscipub.org. This site has full search facilities and e-mail alert options. In the JET specific papers the diagrams contained within the PDFs on this site are hyperlinked

Effects of density gradients and fluctuations at the plasma edge on ECEI measurements at ASDEX Upgrade

B. Vanovac[1], E. Wolfrum[2], S.S. Denk[2], F. Mink[2,4], F. M. Laggner[3], G. Birkenmeier[2,4],M. Willensdorfer[2], E. Viezzer[2,5], M. Hoelzl[2],S. J. Freethy[2], M. G. Dunne[2], A. Lessig[2], N.C. Luhmann Jr. [6], the ASDEX Upgrade Team and the EUROfusion MST1 Team[7]

[1] DIFFER - Dutch Institute for Fundamental Energy Research, Eindhoven, the Netherlands

[2] Max-Planck-Institut für Plasmaphysik, 85748 Garching, Germany

[3] Institute of Applied Physics, TU Wien, Fusion@ÖAW, 1040 Vienna, Austria

[4] Physik-Department E28, Technische Universität München, 85748 Garching, Germany

[5] Department of Atomic, Molecular, and Nuclear Physics, University of Seville, Seville, Spain

[6]Department of Applied Science, University of California at Davis, Davis, CA 95616, USA

[7] See author list of "H. Meyer et al 2017 Nucl. Fusion 57 102014"

E-mail: `B.Vanovac@differ.nl`

July 2017

Abstract. Electron Cyclotron Emission Imaging (ECEI) provides measurements of electron temperature (T_e) and its fluctuations (δT_e). However, when measuring at the plasma edge, in the steep gradient region, radiation transport effects must be taken into account. It is shown that due to these effects, the SOL region is not accessible to the ECEI measurements in steady state conditions and that the signal is dominated by the shine-through emission. Transient effects, such as filaments, can change the radiation transport locally, but cannot be distinguished from the shine-through.

Local density measurements are essential for the correct interpretation of the electron cyclotron emission, since the density fluctuations influence the temperature measurements at the plasma edge. As an example, a low frequency 8kHz mode, which causes 10 % to 15 % fluctuations in the signal level of the ECEI, is analysed. The same mode has been measured with the Lithium Beam Emission Spectroscopy (Li-BES) density diagnostic, and is very well correlated in time with high frequency magnetic fluctuations. With radiation transport modelling of the electron cyclotron radiation in the ECEI geometry, it is shown that the density can largely contribute to the radiation temperature T_{rad} and therefore is in agreement with the experimental observations. The poloidal velocity of the low frequency mode measured by the ECEI is 3km/s. The calculated velocity of the high frequency mode measured on the magnetics is about 25 km/s. Velocities are compared with the $E \times B$ background flow velocity and possible explanations for the origin of the low frequency mode are discussed.

1. Introduction

H-mode plasmas [1], are the foreseen scenario for the ITER operation [2]. This type of scenario is characterized by steep gradients and the pedestal build-up at the edge of the plasma. Edge Localized Modes (ELMs)[3, 4] lead to a periodic relaxations of the gradients including sudden loss of heat and particles into the unconfined region in $\sim$ 1-2 ms time scale. These periodic bursts can cause intolerable heat loads on divertor target plates, and the erosion of plasma facing components. In order to maintain the high confinement of heat and particles, yet with no impurity accumulation and without large uncontrollable ELMs, ELMs need to be mitigated. For such a full control the dynamics of ELMs and ELM associated phenomena must be fully understood.

The Electron Cyclotron Emission Imaging (ECEI) diagnostic, with multiple lines of sight (LOS), where each LOS behaves like a conventional 1D radiometer, measures the radiation temperature and its fluctuations on μs time scales and is specially suitable for 2D or quasi-3D visualisation of MHD phenomena. It can thus help provide more insight into the behaviour of the relative temperature fluctuations associated with the ELM cycle. To date, ECEI has been installed on many tokamaks including: ASDEX Upgrade[5], KSTAR[6], EAST[7], DIII-D[8] and HL-2A[9].

In the case of optically thick plasmas, where optical thickness is proportional to the product of electron density and temperature, the intensity of the cyclotron radiation equals the level of black body emission. In this case, under the condition that the electrons are in a local thermodynamic equilibrium, radiation temperature is equal to the electron temperature. However, when measuring at the plasma edge, where the density and temperatures are relatively low, the electron cyclotron emission no longer equals the black body radiation and the density contribution cannot be neglected. In this case the radiation transport equation is solved in order to obtain the radiation temperatures. It is important to note here that the geometry under which the light is collected, plays a very important role. Under perpendicular observation of the plasma, where the line of sight is perpendicular to the magnetic field line, there is no significant parallel contribution of the cyclotron emission and the Doppler broadening can be neglected. If, however, the observation angle is slightly oblique, as is the case with the present ECEI system on ASDEX Upgrade, this Doppler broadening must be taken into account. In this case the radial resolution of the system is set by both, IF broadening and Doppler broadening. Another important point is related to hot H-mode plasmas where the relativistically down-shifted emission contributes significantly to the low field side emission. This effect shifts the peak of the resonance towards the higher magnetic field [10]. When all the mentioned effects are taken into account, measurement positions in the case of oblique diagnostics can significantly differ from the cold resonances as shown in [11].

In this work, we examine a particular H-mode discharge during the phase between the two subsequent ELM crashes, where the large amplitude density fluctuation alongside with the temperature fluctuations are measured. The main question to answer in this work is if and how much of the fluctuating signal measured with ECEI, which is

considered a temperature diagnostic, is affected by the temporarily varying behaviour of the density.

The paper is organized as follows. The ECEI diagnostic is described in more detail in Section 2. Section 3 explains the forward model that is now routinely used for the ECE Imaging at ASDEX Upgrade. Measurements of the temperature fluctuations and the mode analysis by the ECEI is presented in Section 4. Section 5 treats the spatial localization of the mode. Forward modelling of the EC radiation with density fluctuations in the steep gradient region is described in Section 6. In Section 7 we compare measured mode velocities with the $E \times B$ velocity. Summary is given in Section 8.

2. ECEI at ASDEX Upgrade

The ECEI diagnostic at AUG is well suited for measurements of relative temperature fluctuations with two separate arrays looking at two toroidally separated locations inside the plasma under slightly different toroidal angles [12]. Its poloidal extension enables covering the regions above, across and below the midplane. Figure 1(a) shows the poloidal cross section of ASDEX Upgrade indicating the measurement positions for different edge diagnostics used in this work: ECE Imaging, Li Beam Emission Diagnostic (Li-BES) [13], channels of the 1D ECE radiometer [14] and magnetic pick-up coils . The ECE and ECEI are temperature diagnostics, the Li-BES serves as an edge density profile diagnostic whilst the magnetic pick-up coil measure magnetic fluctuations. The ECEI, ECE and Li-BES are positioned in the same sector of ASDEX Upgrade, therefore measuring at very close toroidal locations. The ECEI has a toroidal observation angle and, when focused at the edge, array 1 has a launching toroidal angle of 7 degrees and array 2 has an angle of 5.7 degrees with respect to the the 1D ECE. The position of the ECEI arrays relative to the 1D ECE radiometer is shown in figure 1(b). As a consequence of the toroidal observation angle, the Doppler broadening of the emission lines is increased, and therefore contributes to the radial resolution of the diagnostic. In this work we use the data from the array 2, whose IF bandwidth is set to 390 MHz for every channel.

Emission of optically thick Maxwellian plasmas, when observed perpendicularly to the magnetic field, originates from a radially thin layer as is the case in the standard ECE diagnostic on ASDEX Upgrade. Therefore, for perpendicular propagation, the radial resolution of the system can be well approximated by the IF bandwidth of the system. ECE Imaging has a contribution of Doppler broadened emission on top of the IF broadening. When observing high density H-mode plasmas under the oblique angle, the LOS can be approximated by a straight line for lower density cases, or bent due to the high density gradient. Refraction of the beams causes an ambiguity in the measurement positions. This is of special importance for the channels at the top and the bottom of the ECEI arrays, since they encounter the strong gradients under the largest angle. Also, due to the high temperature of the plasmas, relativistic effects cannot be neglected. Because

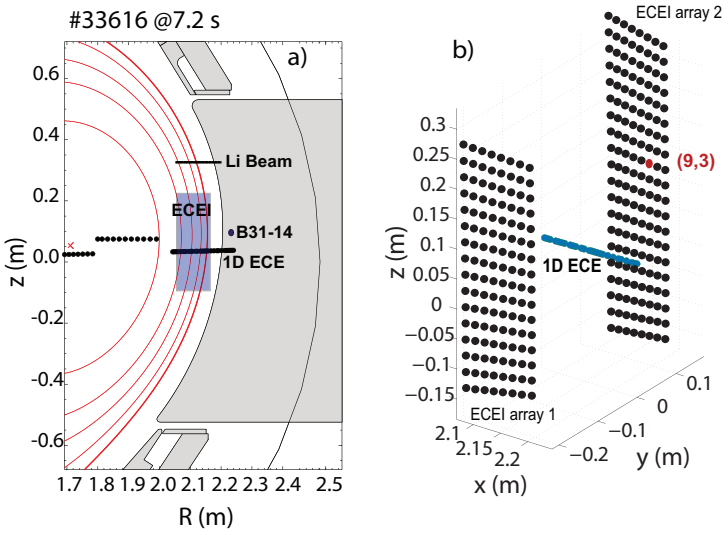

Figure 1: a) Poloidal cross section of ASDEX Upgrade indicating the measurement positions of: the Li beam diagnostic, ECE Imaging, standard ECE radiometer and magnetic pick-up coil (B31-14). b) Measurement positions of two toroidally separated ECEI arrays in black; edge ECE channels in green. A single channel of the ECEI array marked in red is used for comparison with the magnetic measurements.

of the relativistic mass increase of the resonant electrons, the frequency will obey the down shift. When combined with the low optical depth at the plasma edge, these effects make the interpretation and the origin of the electron cyclotron radiation complicated and an extended forward model of the cyclotron radiation (ECFM), including the radiation transport effects, needs to be used as a standard tool for determining the origin of the emitted radiation [11].

3. Forward modelling of the radiation detected by the ECEI

In order to get an idea of the diagnostics constraints and characteristics, we describe the forward modelling of the electron cyclotron radiation for an H-mode discharge where we calculate the expected radiation temperatures for a given equilibrium and electron density and temperature profiles. It is important to note that the IF bandwidth is included in this modelling, the beam is approximated with a single ray and possible influence by the O-mode emission is neglected.

For given T_e and n_e profiles, ray tracing, that accounts for refraction effects, is performed for each channel and then the radiation transport equation is solved along the line of sight until it reaches back to the antenna. The input electron density and temperature profiles are shown in figure 2(a). Ray tracing, with an example of 111.6 GHz channels for all 20 lines of sight, is shown in figure 2(b) alongside the CLISTE equilibrium reconstruction [15]. The separatrix position is shown as solid black line, whilst rays are shown as red dashed lines.

The characteristics of the emitted radiation as calculated by the ECFM of a single ECEI (111.6 kHz) channel at the midplane are given in figure 3. We distinguish two positions describing a single channel. The cold resonance position is only dependent on the magnetic field and is shown as a black dashed line. The emission position changes when radiation transport effects are taken into account and is called warm resonance position. It is shown as a red dashed line. The warm resonance is given by the peak of the birth-place distribution function D_ω, depicted as a blue solid line. The radial resolution of the channel is determined by the width of the D_ω and would correspond to the radial extent of the plasma mostly contributing to the emitted radiation.

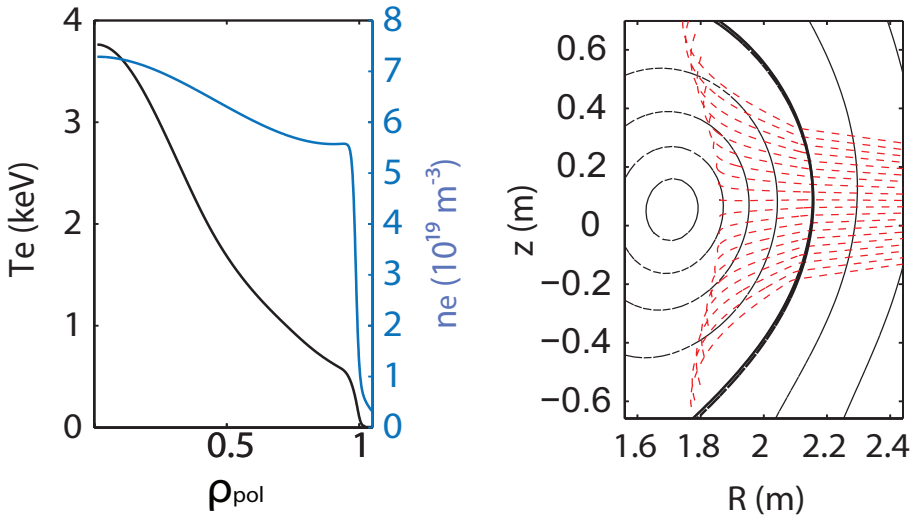

Figure 2: a) T_e and n_e profiles used to forward model the radiation transport. b) Ray tracing representing the lines of sight for 20 ECEI poloidally distributed channels.

The radiation transport equation is solved for every channel of one ECEI array. The two dimensional distribution of the cold and the warm resonances is shown in figure 4(a). It is observed that the inner most channels are Doppler shifted towards the low field side, whilst the outer most channels (with the cold resonances outside the separatrix) are measuring the signal from the region inside the separatrix. This emission corresponds to the relativistically down shifted radiation. Expected radiation temperatures for ECEI channel mapped onto cold and warm resonance positions are shown in figure 4(b) and 4(c), respectively. It is observed that the measured surface area of the ECEI window, when mapped on the warm resonances, is smaller than when mapped onto a cold resonances, due to the shifts mentioned above. In the SOL region only shine-through emission from the pedestal region can be observed in the steady state conditions.

The above analysis shows the effect of steady state plasma conditions on the ECEI measurements. From this, one can conclude that measurements in the SOL region are not feasible with the ECEI diagnostics during steady state, and all the signal measured by channels in the SOL comes from the pedestal top. However, the presence of transient

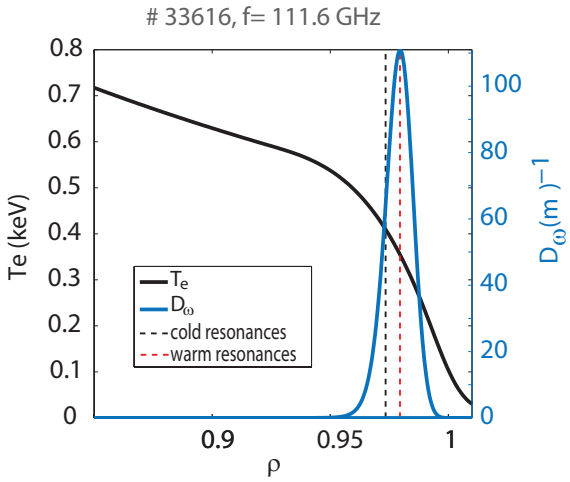

Figure 3: Origin of the observed emission (warm resonance) defined as the peak of the emitted intensity D_ω and the corresponding input T_e profile for the 111.6 GHz ECEI channel, measuring at the midplane. Warm resonance is shown as red dashed line and the cold resonances as black dashed line. The radial width of the plasma contributing to the signal is determined by the width of the D_ω.

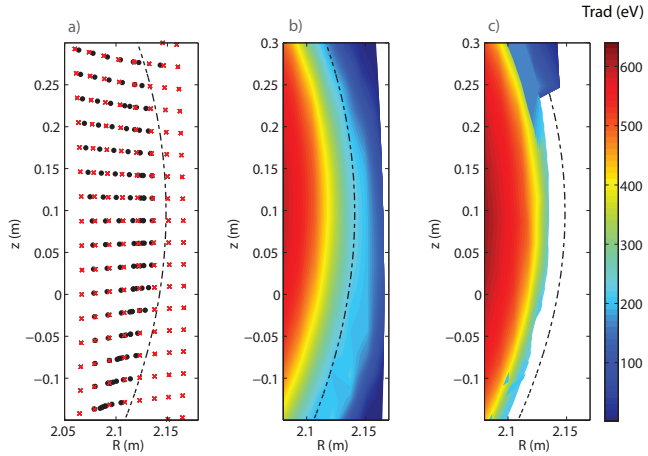

Figure 4: a) Calculated cold resonances (x) and the warm resonances (o) of the ECEI array 1. The radiation temperature mapped onto positions of the cold resonances (b) and the warm resonances (c). The separatrix position is marked by a black dashed line.

events, such as filaments, affects the location of the emitted radiation locally, as shown in figure 5. In order to examine this effect, we use temperature and density distributions from a non-linear JOREK simulation [16] during an ELM crash. These profiles are adjusted to the actual values of the density and the temperature for the shot # 33195 at time t = 2.5872 s and used as an input for ECFM. As shown in figure 5(a) n_e exhibits clear filamentary structures, whilst T_e shown in figure 5(b) is smooth due to fast parallel heat losses on open field lines. The steady state equilibrium is used for this analysis. Modelled cold and warm resonances for these input profiles are shown in figure 5(c)

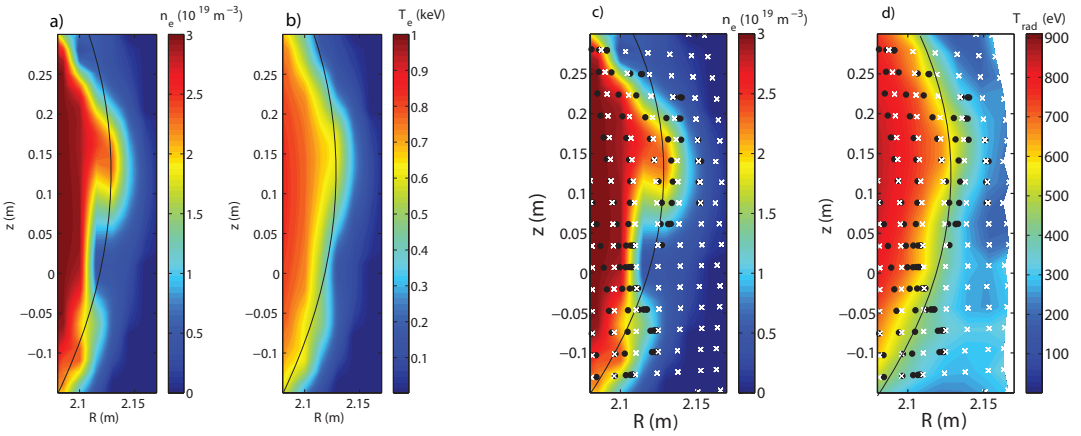

Figure 5: 2D JOREK profiles of a) Electron density; b) electron temperature. These profiles are adjusted to the actual values of the density and the temperature for the shot # 33195 at time t = 2.5872 s and used as an input for ECFM. c) Warm resonance positions as calculated with the ECFM (O) and the cold resonances (X) are mapped onto input density profile (color coded). d)Warm resonance positions as calculated with the ECFM (O) and the cold resonances (X) are mapped onto a radiation temperatures obtained with the forward model for the input electron density and temperature profiles shown in a) and b), respectively.

and 5(d), respectively. In the figure 5(c) cold and the warm resonances are ploted over the input density profile. As seen, the positions of the outermost measurements match with the positions of the filaments. These outermost warm resonances of the LOSs at the midplane are in the SOL region. This shows that the presence of filamentary structures influences the measurement position locally shifting them towards the cold resonances. In figure 5(d), resonant positions are shown together with expected radiation temperature. A shine-through emission is observed. This shine-through originates from the filamentary structures in the SOL region.Although, as shown, it is possible to probe the SOL in non steady state conditions, both T_e and a shine-through is expected in this region. Thus, it makes impossible to correctly interpret the measured signal without the knowledge of the local density fluctuations.

4. Observations of the modes in between an ELM crashes

Less violent transient events related to an ELM are inter-ELM modes. They play a crucial role in understanding an ELM cycle and may also be responsible for transport across the pedestal. So far extensive research on this topic has been reported characterising the dynamics of the temperature fluctuations during the inter-ELM period [17],[18] with ECEI. Magnetic signature also revealed the high frequency fluctuations with well defined mode numbers. They are located in the steep gradient region [19] corresponding to the location of the minimum of the edge radial electric field [20].

Evidence of the quasi-coherent mode during an inter-ELM period have been reported in [21].

In order to obtain an ECEI signal capturing ELM and inter-ELM associated phenomena, measurements are conducted during H-mode plasmas, where steep density and temperature profiles are formed (pedestal). However, to obtain reliable measurements, the cut-off density limit is avoided by focusing on moderate pedestal top density discharges. At the same time the auxiliary heating power is adjusted to obtain ELM frequencies below 100 Hz, so that the inter-ELM dynamics of the temperature fluctuations can be measured.

From the analysis of the previous section, using the typical H-mode profiles shown in figure 2(a), we conclude that radiation temperature equals the electron temperature $T_r = T_e$ and the ECEI system delivers the information on the electron temperature T_e and its fluctuations $\delta T_e/\langle T_e\rangle$ inside the separatrix. Here, $\delta \mathrm{T}_e$ is defined as the $T_e - \langle T_e\rangle$, and $\langle T_e\rangle$ is the time average. An example of the temporal evolution of relative fluctuations of the radiation temperature $\delta T_r/\langle T_r\rangle$ together with the divertor current as ELM indicator in the time period of 60 ms of the discharge # 33616 is given in figure 6(a) and 6(b). Spectrograms of the ECEI signal and the signal measured with the magnetic pick-up coil B31-14, are shown in 6(c) and 6(d), respectively. The discharge was performed at a plasma current I_p = 800 kA, toroidal magnetic field B_t = -2.52 T (negative sign means the opposite to I_p), core line averaged density $\mathrm{n}_e = 7 \times 10^{19}$ m^{-3} and with upper triangularity $\delta_u = 0.128$.

Figure 6(a) shows the temporal evolution of the divertor current. The bursts in the divertor current are correlated with the drop in the relative temperature fluctuations measured with the ECEI channel, shown in 6(b). Recovery of the temperature fluctuations after an ELM crash happens in two steps: fast increase followed by the steady state phase during wich the pressure gradient is clamped. At the onset of the steady phase, a low frequency ($\sim$ 8kHz) narrow band mode sets in, see figure 6(c). The duration of the mode is about 10 ms and vanishes just at the onset of an ELM crash. This low frequency mode correlates well in time with the high frequency modes appearing in the magnetic fluctuation measurements shown in figure 6(d). The toroidal mode numbers of the high f modes, determined from the magnetics are -8, -9, -10 showing that there are multiple modes present in this frequency region. The negative sign corresponds to the rotation of the mode in the electron diamagnetic direction.

A closer look at the inter-ELM mode is taken in figure 7. The measurement positions of the edge ECEI channels are shown in figure 7(a). All channels distributed along the flux surface, marked as red crosses see the 8kHz mode that modulates the temperature fluctuation level up to 10 % - 15 %.

The temporal evolution of the temperature fluctuations measured by the single ECEI channel at the vertical position z = 0.1 m, corresponding to the magnetic midplane, is shown in figure 7(b). A spectrogram of the midplane measurement, presented in figure 7(c), shows the strong mode in the $\sim$ 8 kHz range. The observed mode slightly changes in frequency during its lifetime. The duration of the mode is $\sim$

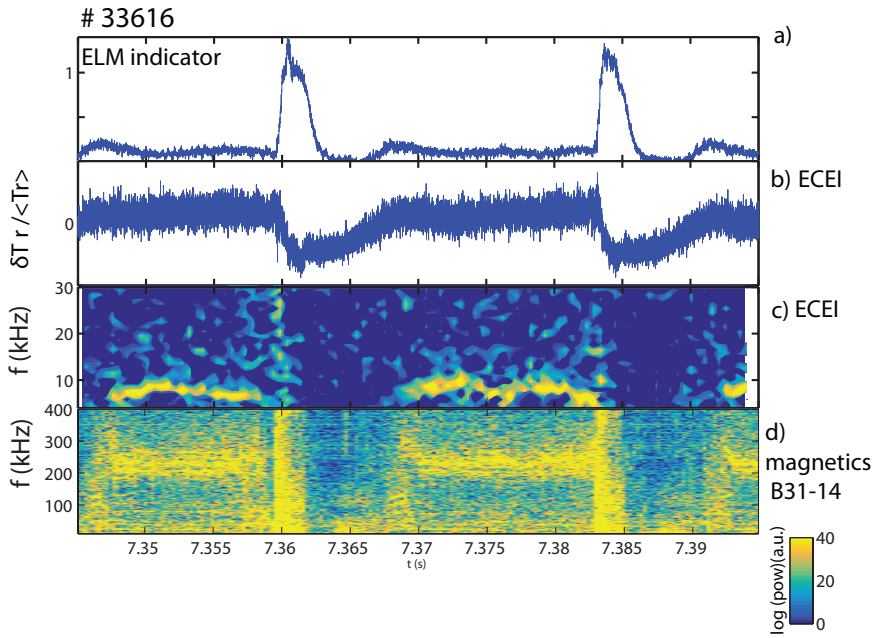

Figure 6: Shot # 33616. Temporal evolution of the: a) Divertor current. b) Radiation temperature fluctuations δ T$_r/\langle T_r \rangle$ measured by the single ECEI channel in the steep gradient region. Power spectral density comparison between:c) ECEI channel; d) magnetic pick-up coil. Position of both ECEI channel and the magnetic coil are indicated in figure 1.

10 ms and the measured absolute fluctuation level during the lifetime of the mode is about 10 %.

Poloidally resolved measurements of the temperature fluctuations expressed in percentage along the flux surface are shown in figure 7(d) in a form of vertically distributed time traces. This kind of visualisation helps to follow the propagation direction of the mode. From here it can be seen that the mode propagates from the bottom to the top, corresponding to the electron diamagnetic direction.

Such poloidally resolved measurements enable the determination of the poloidal velocity of the observed mode. Figure 8(a) is a zoom into the phase of constant frequency of the mode. Three channel at the midplane (z=0) are set to zero. The quality of data was too poor due to electronics, therefore are omitted for better graphical representation.

In order to determine the velocity of the mode in the vertical plane we use the cross correlation between a reference channel and all the other poloidally distributed channels along the flux surface as shown in figure 8(b). The velocity measured this way, shows no variations along the flux surface, and follows the straight line as indicated by the black arrow. The calculated velocity of the mode is $\sim$ 3 km/s moving in the electron diamagnetic direction. Cross correlation between three vertical positions indicates the structure with three maxima fitting in the ECEI observation window. The local poloidal wavelength of this mode, as measured on the low field side, therefore is $\lambda_{pol} \sim 15$ cm.

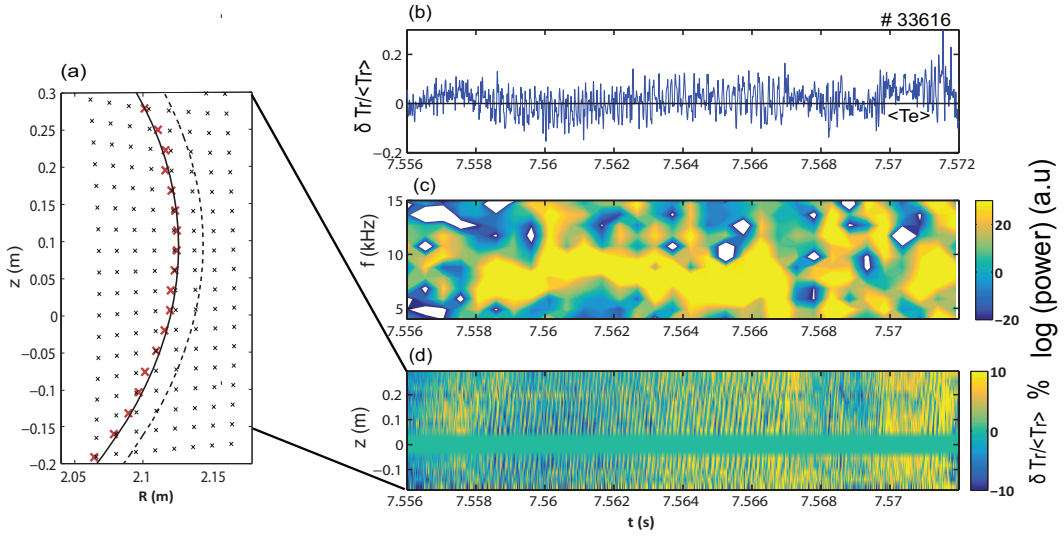

Figure 7: Localization and the temporal evolution of the T_r fluctuations seen in the ECEI observation window. a) Warm resonant channels (red crosses) of the array 2 distributed along the flux surface at $\rho_{pol} \sim 0.985$. (b) Fluctuation level of a single channel 10 cm above the midplane. c) Time resolved spectrogram of the channel as in (b) showing the presence of the strong mode in the 7 - 8 kHz range. d) Temporal evolution of the fluctuation level in percentage measured by the channels with positions shown in (a) as red crosses. This allows to track the propagation of the fluctuations in the poloidal direction, from the bottom to the top channels, along the flux surface. Three channel at the midplane (z=0) are set to zero.

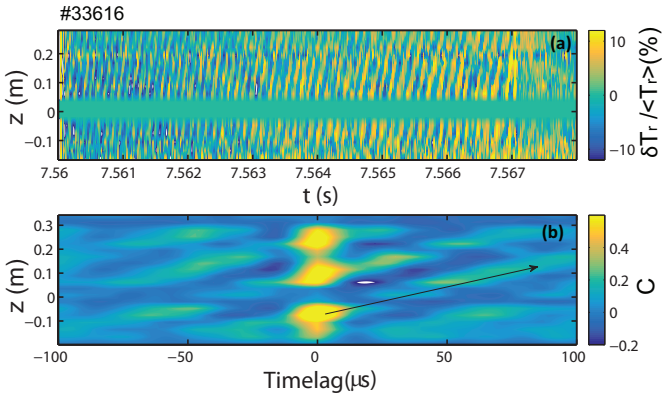

Figure 8: a) Vertically resolved temperature fluctuations along the flux surface during the 8 kHz mode duration. (b) Cross-correlation of the reference channel taken at the vertical position z = -0.1 m with all other poloidal channels. The black arrow approximates the direction of the mode propagation in space and time. From here we can obtain the vertical velocity of the mode.

5. Spatial localization

To complement the analysis of the modes observed with the ECEI, data is compared with other edge diagnostics shown in figure 1(a). The Li-BES diagnostic that resolves the profiles of the electron density and its fluctuations at the plasma edge also observed the mode activity. It is also measured by the conventional 1D ECE radiometer. Comparison between conventional ECE, ECE Imaging and Li-BES measurements at the edge is shown in figure 9 in the form of spectrograms. All spectrograms show activity in the $\sim$ 8kHz range indicating the mode is present in both, density and temperature measurements.

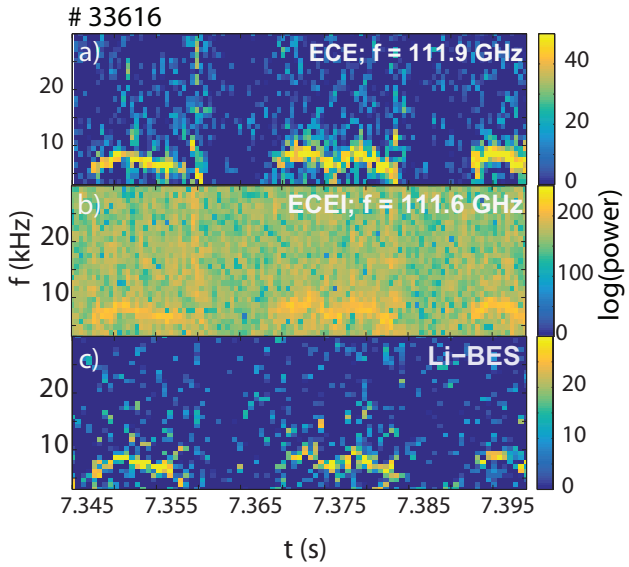

Figure 9: Power spectral density showing a narrow band mode; a) in the ECE channel, b) ECEI, c) Li beam channel

Measurements of the Li-BES diagnostics enabled the access to the amplitude of the density fluctuations. The amplitude of the density fluctuations is estimated from the Li-BES forward model [13] in the following fashion: In order to obtain the information on the amplitude of the density fluctuation $\delta n/n$, this quantity is varied in order to match measured fluctuations in the collected light $\delta I/I$ of 10 %. The perturbation is assumed to be Gaussian, of the width that matches the radial resolution of the Li-BES system (5 mm). The location of the perturbation (center of the Gaussian) matches the channel where the mode is detected. The density fluctuation level obtained this way is between 20 % - 40 %. The background electron density at the position of the mode is between $(4-5)\times10^{19}$ m^{-3}.

Li-BES and 1D ECE radial resolution of 5 mm allows for more accurate localisation of the mode than the one from the ECEI. The 1D ECE channel at the same location as the Li-BES channel measure the mode activity therefore the position of the measurement corresponds to the position of its respective channels at $\rho_{pol} = 0.983$. At the separatrix position at $\rho_{pol} = 1$ mode is not observed, whilst at the location $\rho_{pol} = 0.97$ and inwards,

ECE and ECEI do not observe the mode. Li-BES diagnostic is not sensitive in this region.

This information is further used in the forward model of the electron cyclotron emission in order to investigate the influence of the density perturbation on the signal measured by the ECEI in the steep gradient region where the mode is measured.

6. Forward model of the EC radiation with density fluctuations

The limits of the density perturbation level are estimated as explained in the previous section. From the Li-BES forward model, the upper limit in the density fluctuation amplitude is set to 40 %.

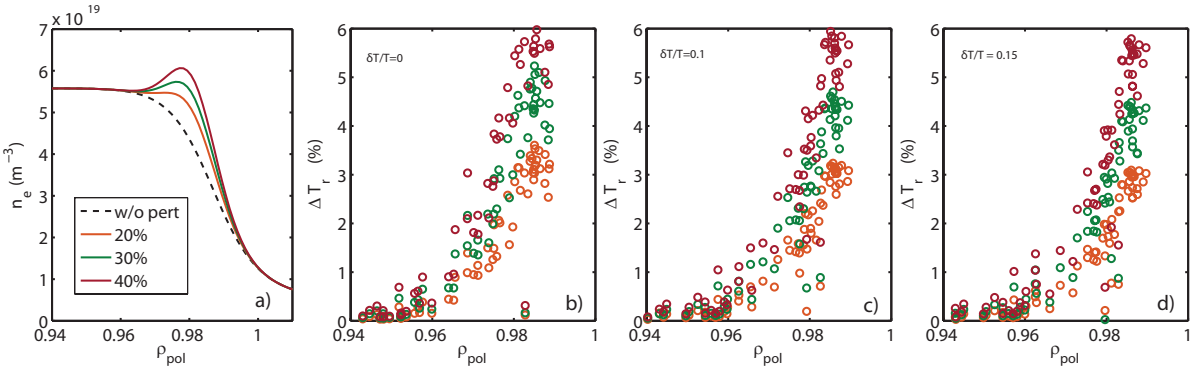

Figure 10: Radiation temperatures (ΔT_r) in percentage defined as $\Delta T_r = \delta T_r / \langle T_r \rangle$ obtained by the ECFM for the different levels of the density perturbations as shown in a). b) Radiation temperatures without input temperature perturbation. c) with input temperature perturbation of 10 %. d) with the input temperature perturbation of 15 %.

In order to model the response of the radiation temperature to the density fluctuation level, the same steps as explained in section 3 are applied. This study requires the input profiles with inserted density perturbation that mimics the one measured by the Li-BES diagnostic. The shape of the perturbationis the same one used in the Li-BES forward model.

Modelling accounts for three different scenarios assuming that we have the cases where the temperature and the density are perturbed at the same time. For this reason the input electron temperature profile $\delta T/T$ is set to 0, 0.1, 0.15, respectively. For each case we varied the density perturbation level as shown in figure 10.

Figure 10 (a) shows the input density profiles used for the modelling. The perturbation level is varied from 20 - 40 % and is color-coded.

Variations in the radiation temperatures cannot be distinguished between the three cases for $\delta T_e/T_e$ of 0, 0.1, 0.15 shown in figure 10(a), 10(b), 10(c), respectively. Contrary to that, the density perturbation level $\delta n_e/n_e$ for each particular case changes the

absolute change in the radiation temperature ΔT_r. At the location of the mode ($\rho_{pol} = 0.983$) we can see that the 20 % of the density perturbation is captured in the radiation temperatures inducing 3 % absolute change in the radiation temperature. Absolute change in the T_r increases with the amplitude of the density fluctuations. It is important to note that in the forward model we omitted the possible O-mode contribution and the complex ECEI beams are approximated with a single array. This already simplifies the complexity of the ECEI geometry, therefore the modelled and measured amplitudes cannot be directly compared.

7. Mode velocities and comparison to the $\mathbf{v}_{E\times B}$ velocity

The mode velocity in the ECEI reference frame is $v_{mode} = v_{E\times B} + v_{ph}$, where $v_{E\times B}$ is governed by the radial electric field E_r at the location of the mode, and v_{ph} is the intrinsic phase velocity of the mode. The E_r profile for this discharge is estimated using the neoclassical approximation for the poloidal flow of main ions[22], using experimental profiles of n_e and T_i. The n_e and reconstructed E_r profiles are shown in figure 11(a).The position of the mode detected with different diagnostics is within the color coded areas that represent radial extent of the plasma contributing to measurements. Gray corresponds to the radial resolution of the ECEI and red to the Li-BES and ECE, respectively. It can be seen that the ECEI averages the signal over a much wider range of plasma radius. However, the radial resolution of the Li-BES and ECE enabled localization of the mode to a precision of up to 5 mm as explained in the Section 5. The background $v_{E\times B}$ velocity is calculated as $v_{E\times B}(r) = \frac{\vec{E(r)}\times\vec{B(r)}}{B(r)^2}$ and is shown in figure 11 (b).

The evaluated $\mathrm{v}_{E\times B}$ at the position of the mode is about 25 km/s and matches with the minimum of the E_r. This is, however, not in agreement with the velocity obtained from the ECEI diagnostic, which is measured to be 3 km/s.

The high frequency modes (see figure 6(d)) are observed at the same time as the low frequency modes on the magnetic pick-up coils measuring at the low field side. As shown in [20] the high frequency modes measured by the pick-up coils are located in the minimum of the E_r - at the same location as the low frequency modes measured by the ECEI. From the measured frequency of the high frequency modes, if the mode is located on the rational surface $q = \frac{m}{n}$, one can determine its poloidal velocity as the $v_{mode} = 2\cdot\pi\cdot r\frac{f}{q\cdot n}$, where r is the radial location of the mode and f its frequency. Using the following parameters of $q = 5$, $f = 240$ kHz, $n = 8$ and $r = 0.6$ m, the calculated mode velocity is $\sim$ 22 km/s and is comparable with the $E \times B$ velocity within the measurement uncertainties. Although the propagation direction of both low and the high frequency modes is in the electron diamagnetic direction and they exist at the same radial location, velocities of those modes differ by almost a factor of 10.

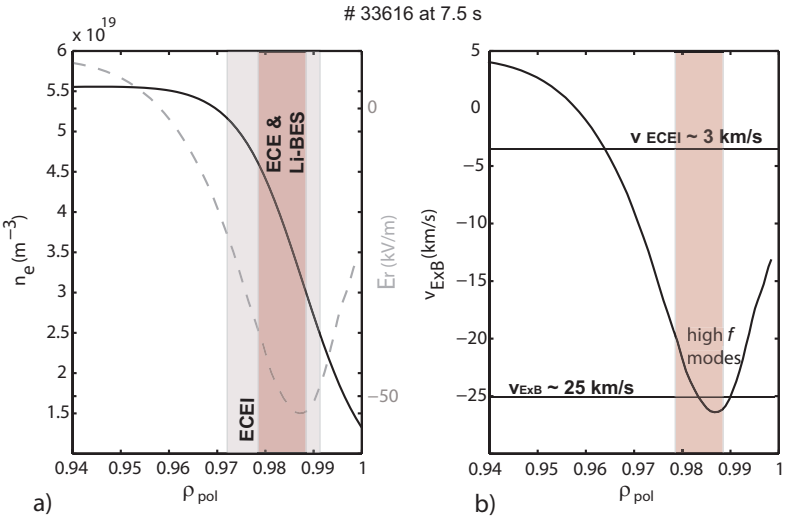

Figure 11: Shot # 33616 at t= 7.5 s. a) Density profile of the steep gradient edge region shown as a black solid line; radial electric field E_r estimated from the poloidal flow of impurities is presented as a dashed gray line. Radial resolution of the edge diagnostics used in this work is color coded: red corresponding to the Li-BES and 1D ECE channel; grey corresponding to the ECEI channel. b) $E \times B$ velocity calculated using the E_r. The red shaded area shows corresponds to the measured low f and high f modes.

8. Summary and Discussion

In summary, it is shown that SOL measurements with the ECEI are not feasible in steady state due to the shine-through emission in this region. The radiation temperature in the SOL region, which is a region of low optical depth, is down-shifted emission from the electrons in the tail of the Maxwellian originating in the pedestal region.

However, the presence of ELM filaments in the SOL region can change the optical depth locally, due to the locally higher density and temperature, therefore both, shine-through as well as the local emission can be observed simultaneously. Since both, T_e and T_r are measured in this region, it is difficult to distinguish between the two contributions without the local density measurements.

In the H-mode discharge examined in this work, a strong 8 kHz mode has been observed with different edge diagnostics between ELMs. The mode is highly correlated with the high frequency ($\sim$ 200 kHz) inter-ELM modes detected on the magnetic pick-up coils. The cross-correlation analysis from the ECEI measurements has shown the poloidal structure of the mode with the local poloidal wavelength $\lambda_p = 15$ cm. The poloidal mode velocity as calculated from the ECEI channels distributed along the flux surface is 3 km/s in the electron diamagnetic direction. High spatial resolution of the Li-BES and 1D ECE enabled localization of the 8 kHz mode with higher accuracy than the one of the ECEI showing the mode in the steep gradient region corresponding to the

minimum of the radial electric field. The same 8 kHz mode in between ELMs is observed in the density measurements with the Li-BES diagnostic. Since measurements of the Li-BES are sensitive to the changes in the density it is concluded that n_e fluctuations contribute to the ECEI measurements. To account for this we used forward model of the electron cyclotron emission by adding a Gaussian perturbation in the pedestal region to mimic the possible density fluctuations in that region. This study has shows that the density fluctuation level can influence the measurements of ECEI and contribute to the measured radiation temperature T_r. Thus, knowledge about the local density values is necessary for correct interpretation of the measured signal.

Further more, we have shown measurements of the ECEI's low frequency mode setting in the phase of the clamped pressure gradient before an ELM crash. This low frequency mode appears also in other diagnostic alongside multiple high frequency modes detected in the magnetic pick-up coil. As shown, the propagation direction of both low and the high frequency modes is in the electron diamagnetic direction, in agreement with the sign of the radial electric field in that region and are at the same radial location. The magnetic pick-up coils measure multiple modes with well defined toroidal mode numbers whilst the ECEI/ECE/Li-BES measures a single mode at low frequency. The low frequency mode is also seen on the magnetics, but of very low amplitude and its mode numbers remained undetermined.

This opens up the hypotheses about the origin of the low frequency mode: One hypothesis supports the idea of having an interaction between two or more high frequency modes that as a result give the low frequency mode. This resulting mode is non linearly amplified in the low field side region where it is measured by the ECEI. Experimental findings that support this theory have already been reported on different machines. Significant modification of the mode structure due to the non-linear coupling has been reported on TCV [23] and similar amplitude modulation has been observed in KSTAR [24] and explained by a superposition of two modes with different poloidal velocities. In the case studied in this work, the result of the multiple mode interaction would be the wave with a measured group velocity of 3 km/s.

Another hypothesis is that the measured mode is a mode for itself coexisting together with the high frequency modes, at the same position, but very weak in amplitude compared to the high frequency modes. In this case, the $E \times B$ velocity of 25 km/s and the measured mode velocity of 3 km/s would result in a mode with a large phase velocity $v_{ph} = 22$ km/s, in the ion diamagnetic direction.

To distinguish between the possible explanations on the origin of the mode in near future work we will examine the poloidal velocities of the low frequency modes with a variation of plasma parameters which are known to change the frequency of the high frequency modes, i.e. edge safety factor q and the ion pressure gradient ∇p_i. Also, will compare the dynamics of the fluctuations measured by the ECEI with newest non-linear JOREK simulation comprising an inter-ELM period.

The ECEI diagnostic is a useful tool for characterizing fluctuations at the edge by means of their poloidal size and velocity, the signal, however, can be dominated by the

changes in the density profile and does not necessarily reflect the amplitude of the T_e fluctuations.

Acknowledgements

This work has been carried out within the framework of the EUROfusion Consortium and has received funding from the Euratom research and training programme 2014-2018 under grant agreement No 633053. The views and opinions expressed herein do not necessarily reflect those of the European Commission.

[1] F. Wagner, G. Becker, K. Behringer, D. Campbell, A. Eberhagen, W. Engelhardt, G. Fussmann, O. Gehre, J. Gernhardt, G. v. Gierke, G. Haas, M. Huang, F. Karger, M. Keilhacker, O. Klüber, M. Kornherr, K. Lackner, G. Lisitano, G. G. Lister, H. M. Mayer, D. Meisel, E. R. Müller, H. Murmann, H. Niedermeyer, W. Poschenrieder, H. Rapp, H. Röhr, F. Schneider, G. Siller, E. Speth, A. Stäbler, K. H. Steuer, G. Venus, O. Vollmer, and Z. Yü. Regime of improved confinement and high beta in neutral-beam-heated divertor discharges of the ASDEX tokamak. *Phys. Rev. Lett.*, 49:1408–1412, Nov 1982.

[2] Y R Martin, T Takizuka, and the ITPA CDBM H-mode Threshold Database Working Group. Power requirement for accessing the h-mode in ITER. *Journal of Physics: Conference Series*, 123(1):012033, 2008.

[3] H. Zohm. Edge localized modes (ELMs). *Plasma Physics and Controlled Fusion*, 38(2):105, 1996.

[4] A. W. Leonard. Edge-localized-modes in tokamaks. *Physics of Plasmas*, 21(9):090501, 2014.

[5] I. G. J. Classen, J. E. Boom, W. Suttrop, E. Schmid, B. Tobias, C. W. Domier, N. C. Luhmann Jr., A. J. H. Donné, R. J. E. Jaspers, P. C. de Vries, H. K. Park, T. Munsat, M. Garcia-Munoz, and P. A. Schneider. 2D electron cyclotron emission imaging at ASDEX upgrade (invited). *Review of Scientific Instruments*, 81(10):10D929, 2010.

[6] G. S. Yun, W. Lee, M. J. Choi, J. Lee, M. Kim, J. Leem, Y. Nam, G. H. Choe, H. K. Park, H. Park, D. S. Woo, K. W. Kim, C. W. Domier, N. C. Luhmann Jr., N. Ito, A. Mase, and S. G. Lee. Quasi 3D ECE imaging system for study of MHD instabilities in KSTAR. *Review of Scientific Instruments*, 85(11):11D820, 2014.

[7] L Yu, C W Domier, X Kong, S Che, B Tobias, H Park, C X Yu, and N C Luhmann Jr. Recent advances in ECE imaging performance. *Journal of Instrumentation*, 7(02):C02055, 2012.

[8] B. Tobias, C. W. Domier, T. Liang, X. Kong, L. Yu, G. S. Yun, H. K. Park, I. G. J Classen, J. E. Boom, A. J. H. Donné, T. Munsat, R. Nazikian, M. Van Zeeland, R. L. Boivin, and N. C. Luhmann Jr. Commissioning of electron cyclotron emission imaging instrument on the DIII-D tokamak and first data. *Review of Scientific Instruments*, 81(10):10D928, 2010.

[9] M. Jiang, Z. B. Shi, S. Che, C. W. Domier, N. C. Luhmann Jr., X. Hu, A. Spear, Z. T. Liu, X. T. Ding, J. Li, W. L. Zhong, W. Chen, Y. L. Che, B. Z. Fu, Z. Y. Cui, P. Sun, Y. Liu, Q. W. Yang, and X. R. Duan. Development of electron cyclotron emission imaging system on the hl-2A tokamak. *Review of Scientific Instruments*, 84(11):113501, 2013.

[10] B. J. Tobias, M. E. Austin, J. E. Boom, K. H. Burrell, I. G. J. Classen, C. W. Domier, N. C. Luhmann Jr., R. Nazikian, and P. B. Snyder. Ece-imaging of the h-mode pedestal (invited). *Review of Scientific Instruments*, 83(10):10E329, 2012.

[11] Denk, Severin S., Fischer, Rainer, Maj, Omar, Poli, Emanuele, Stober, Jrg K., Stroth, Ulrich, Vanovac, Branka, Suttrop, Wolfgang, Willensdorfer, Matthias, and ASDEX Upgrade Team. Radiation transport modelling for the interpretation of oblique ece measurements. *EPJ Web Conf.*, 147:02002, 2017.

[12] I. G. J. Classen, C. W. Domier, N. C. Luhmann Jr., A. V. Bogomolov, W. Suttrop, J. E. Boom, B. J. Tobias, and A. J. H. Donné. Dual array 3D electron cyclotron emission imaging at ASDEX upgrade. *Review of Scientific Instruments*, 85(11):11D833, 2014.

[13] M Willensdorfer, G Birkenmeier, R Fischer, F M Laggner, E Wolfrum, G Veres, F Aumayr, D Carralero, L Guimaris, B Kurzan, and the ASDEX Upgrade Team. Characterization of the Li-BES at ASDEX upgrade. *Plasma Physics and Controlled Fusion*, 56(2):025008, 2014.

[14] W. Suttrop and A.G. Peeters. Practical limitations to plasma edge ewlectron temperature measurements by radiometry of electron cyclotron emission. *IPP report*, 1996.

[15] P J Mc Carthy and ASDEX Upgrade Team. Identification of edge-localized moments of the current density profile in a tokamak equilibrium from external magnetic measurements. *Plasma Physics and Controlled Fusion*, 54(1):015010, 2012.

[16] G.T.A. Huysmans and O. Czarny. MHD stability in x-point geometry: simulation of ELMs. *Nuclear Fusion*, 47(7):659, 2007.

[17] I.G.J. Classen, J.E. Boom, A.V. Bogomolov, E. Wolfrum, M. Maraschek, W. Suttrop, P.C. de Vries,

A.J.H. Donné, B.J. Tobias, C.W. Domier, N.C. Luhmann, and the ASDEX Upgrade Team. The role of temperature fluctuations in the dynamics of type-I and type-ii edge localized modes at ASDEX upgrade. *Nuclear Fusion*, 53(7):073005, 2013.

[18] J.E. Boom, I.G.J. Classen, P.C. de Vries, T. Eich, E. Wolfrum, W. Suttrop, R.P. Wenninger, A.J.H. Donné, B.J. Tobias, C.W. Domier, N.C. Luhmann Jr, H.K. Park, and the ASDEX Upgrade Team. 2D ECE measurements of type-I edge localized modes at ASDEX upgrade. *Nuclear Fusion*, 51(10):103039, 2011.

[19] Felician Mink, Elisabeth Wolfrum, Marc Maraschek, Hartmut Zohm, Lszl Horvth, Florian M Laggner, Peter Manz, Eleonora Viezzer, Ulrich Stroth, and the ASDEX Upgrade Team. Toroidal mode number determination of ELM associated phenomena on ASDEX upgrade. *Plasma Physics and Controlled Fusion*, 58(12):125013, 2016.

[20] F M Laggner, E Wolfrum, M Cavedon, F Mink, E Viezzer, M G Dunne, P Manz, H Doerk, G Birkenmeier, R Fischer, S Fietz, M Maraschek, M Willensdorfer, F Aumayr, the EUROfusion MST1 Team, and the ASDEX Upgrade Team. High frequency magnetic fluctuations correlated with the inter-elm pedestal evolution in ASDEX upgrade. *Plasma Physics and Controlled Fusion*, 58(6):065005, 2016.

[21] A. Diallo, R. J. Groebner, T. L. Rhodes, D. J. Battaglia, D. R. Smith, T. H. Osborne, J. M. Canik, W. Guttenfelder, and P. B. Snyder. Correlations between quasi-coherent fluctuations and the pedestal evolution during the inter-edge localized modes phase on DIII-D. *Physics of Plasmas*, 22(5):056111, 2015.

[22] E. Viezzer, T. Pütterich, G.D. Conway, R. Dux, T. Happel, J.C. Fuchs, R.M. McDermott, F. Ryter, B. Sieglin, W. Suttrop, M. Willensdorfer, E. Wolfrum, and the ASDEX Upgrade Team. High-accuracy characterization of the edge radial electric field at asdex upgrade. *Nuclear Fusion*, 53(5):053005, 2013.

[23] R.P. Wenninger, H. Reimerdes, O. Sauter, and H. Zohm. Non-linear magnetic perturbations during edge-localized modes in TCV dominated by low n mode components. *Nuclear Fusion*, 53(11):113004, 2013.

[24] M. Kim, J. Lee, H.K. Park, G.S. Yun, W. Lee, C.W. Domier, Luhmann N.C. Jr., and KSTAR team. Multimode excitation during the inter-ELM crash periods in KSTAR h -mode plasma. *Nuclear Fusion*, 55(7):073001.